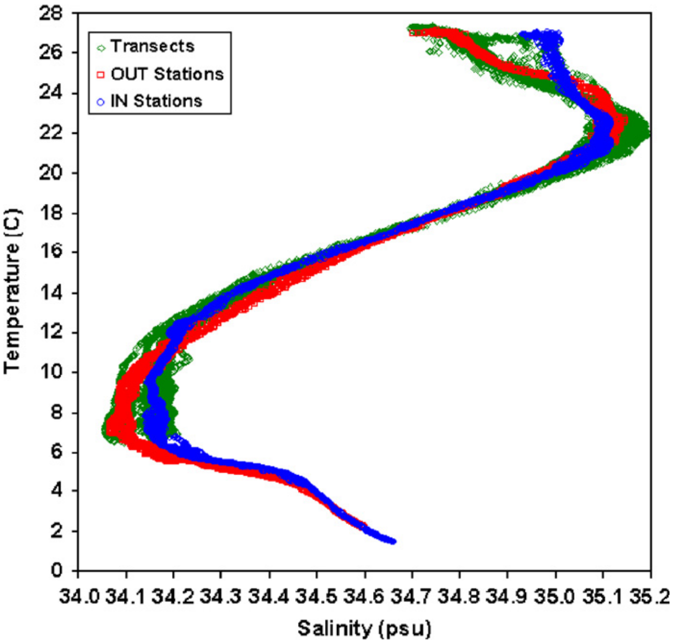

Fig. 4. Temperature–salinity (*T*–*S*) relationship for all IN- (blue), OUT- (red), and STAR- stations (green).

in the hydrography. However, significant positive differential chlorophyll *a* anomalies were centered at ~75 m depth and spanned 50 km horizontally (Fig. 5A; Transect 2).

Dissolved-oxygen concentrations from both transect lines showed enhanced concentrations well above the DCML and sigma-$t = 24\,kg\,m^{-3}$ isopycnal layer (Fig. 5B). Relatively elevated oxygen concentrations followed the sigma-$t = 23\,kg\,m^{-3}$ isopycnal at depths between 50 and 75 m, spanning ~80 km horizontally near the center. Differential oxygen anomalies (Fig. 5B) confirm concentrations were enhanced in the surface layer at ~50 m, above the differential density anomaly and subsurface chlorophyll *a* maximum, while negative DPA's were found deeper (~125 m). Just below the positive differential density anomaly near the eddy center, negative oxygen anomalies ($-0.40\,mg\,L^{-1}$) spanning ~60 km are present (Fig. 5B). The negative oxygen anomalies are similar in magnitude and location to the negative chlorophyll *a* anomalies shown in Fig. 5A.

The northwest to southeast (Transect 3) vertical sections of dissolved inorganic nitrate+nitrite (NO_3+NO_2), phosphate (PO_4) and silicic acid ($Si(OH)_4$) are shown in Fig. 6 along with their respective differential anomalies. Comprehensive biological–biogeochemical sampling was conducted only during Transect 3. These vertical sections were not derived from the same high-resolution profiles as for chlorophyll *a* and oxygen concentrations, since nutrient concentrations were measured from water samples collected at discrete depths. Relatively deep nutrient doming was evident at 175 m depth (below the euphotic zone and DCML). Doming was roughly congruent with the sigma-$t = 24.5\,kg\,m^{-3}$ density layer (Fig. 2C). Differential nitrate+nitrite and phosphate anomaly contour plots show enhanced concentrations near the center of *Noah* just below the positive differential density anomalies at 150 m depth. Silicic acid contours also show nutrient enrichment on isopycnal surfaces similar to those for nitrate+nitrite and phosphate, but these are skewed slightly to the northwest region of the transect line. STAR-station 20 (Cast 29) shows that enhanced silicic acid concentrations extended up to depths of 50 m. The differential silicate anomaly confirms that enhanced concentrations are present to the northwest of the eddy center below the euphotic layer. High DPA values above the 1% light level at 40 km along Transect 3 reflect the presence of high concentrations at shallower depths observed during STAR-station 20. Silicic acid-to-nitrate+nitrite ratios within the eddy feature ($Si(OH)_4$:N+N) did show decreases at <250 m depths relative to the OUT_{AVG} stations. The lack of positive macronutrient anomalies above the 1% light level near the sub-surface core of *Noah* indicates that nutrient depletion and possibly nutrient limitation may have occurred or was still occurring.

Mean vertical profiles of nitrate+nitrite, phosphate, silicic acid, and oxygen to 1000 m depth for the IN_{AVG} and OUT_{AVG} stations are shown in Fig. 7. Although concentrations of inorganic nutrients are slightly higher at respective depths in the euphotic layer (>100 m), large deviations relative to the OUT_{AVG} stations are not prevalent until depths below 200 m; thus, the profile figures are expanded to include deeper depths (Figs. 6 and 7). This trend is particularly evident in the silicic acid profile where IN_{AVG} versus OUT_{AVG} stations show relatively small differences to 250 m depth. The vertical displacements of physical properties found in Fig. 3 are more dramatic than the shifts of biogeochemical properties suggesting that the nutrients may have already been utilized within the euphotic layer during the survey. This difference could be another indication that the eddy, from a biological–biogeochemical perspective, may have been in a decay phase (similarly reported for Cyclone *Opal* by Rii et al., 2008). IN_{AVG} and OUT_{AVG} oxygen profiles reveal that the oxygen maximum shoals from below 100 m to depths of about 75 m. The perturbation in the oxygen profile extends only to 500 m depth, indicating that the uplift associated with *Noah* was moderate during the E-Flux I experiment. Despite the relatively shallow shoaling of isopleths, the nutrient data suggest that the chemical structure is manifest at much greater depths of between ~250 and 1000 m. The largest deviation between IN_{AVG} and OUT_{AVG} stations occurs between the depths of 500–700 m and converges at a depth of 1000 m. Based on these chemical structure results, it is highly plausible that *Noah's* physical isopycnal doming may have occurred to much greater depths during an earlier phase of its life cycle.

3.3. Velocity distributions

ADCP horizontal current velocity vectors at 40 m depth (shallowest ADCP depth record) are shown in Fig. 8 for all transects. The figure was generated by translating the transects into a reference frame with a common eddy center as determined for Transect 3. Current vector data clearly reaffirm the presence of the mesoscale cyclonic feature *Noah* west of the island of Hawai'i. Velocities associated with the eddy of up to $80\,cm\,s^{-1}$ were observed along the northern and southern section of Transect 2 (Fig. 8; top). The velocity vector fields show currents that gradually decrease in magnitude to about 200 m depth (not shown), indicating that the vertical influence of the velocity field associated with the cyclonic feature is much shallower than the eddy-induced perturbations observed in the hydrographic and biogeochemical data. Current velocities are generally slower nearer the coastline of Hawai'i (southeastern section of Transect 3). In addition, a small anti-cyclonic pattern is evident in the case of the northeastern section of Transect 4, likely resulting from channel and coastal island effects.

In order to represent better the entirety of the eddy feature, ADCP transect data were interpolated (Kriging method) at 40 m depth (Fig. 8; bottom). The horizontal interpolation of current vectors shows the individual transect lines of a well-developed cyclonic circulation feature with pronounced jet-like regions in the northern (near the channel) and southwestern (furthest from the channel) portions. Maximum velocity of $86\,cm\,s^{-1}$ was recorded in the southwestern region during Transect 1 at 40 m